Transport properties of single-wall carbon nanotube Y junctions

Antonis N. Andriotis,[1,*] Madhu Menon,[2,3,†] Deepak Srivastava,[4,‡] and Leonid Chernozatonskii[5,§]
[1]*Institute of Electronic Structure and Laser, Foundation for Research and Technology-Hellas, P.O. Box 1527, 71110 Heraklio, Crete, Greece*
[2]*Department of Physics and Astronomy, University of Kentucky, Lexington, Kentucky 40506-0055*
[3]*Center for Computational Sciences, University of Kentucky, Lexington, Kentucky 40506-0045*
[4] *NASA Ames Research Center, CSC, Mail Stop T27-A1, Moffett Field, California 94035-1000*
[5]*Institute of Biochemical Physics, Russian Academy of Sciences, Moscow 117977, Russian Federation*
(Received 20 November 2001; published 5 April 2002)

Quantum conductivity of a wide class of carbon nanotube Y junctions is calculated using an efficient Green's function embedding scheme. Our results indicate that rectification and switching properties of these junctions depend strongly on the symmetry and to a lesser degree on chirality. We find that a zig-zag tube forming the stem of a symmetric Y junction is sufficient to cause perfect rectification across the junction, otherwise the *I-V* characteristics remain asymmetric with some leakage current for positive bias voltages. For asymmetric Y junction, on the other hand, we find that no rectification at all is possible. We invoke a model calculation involving Y branching in molecules as well as in nanotubes to explain the dependence of rectification on the nature of the geometry at the branching.

DOI: 10.1103/PhysRevB.65.165416 PACS number(s): 73.50.−h, 73.23.Hk, 73.61.Wp

I. INTRODUCTION

The carbon nanotube junctions have recently emerged as excellent candidates for use as building blocks in the formation of nanoscale electronic devices. The discovery of localized bends in multiwalled pure carbon nanotubes[1] has inspired theoretical investigations of simple two-point tube junctions in single-walled tubes.[2–5] If such a heterojunction is formed by two nanotubes, one semiconducting and the other metallic, the junction will function like a rectifying diode. The two-terminal rectifying devices, however, lack the versatility of the three-terminal devices where the third terminal could be used for controlling the switching mechanism, power gain, or other transisting applications that are needed in any extended molecular electronic circuit.

Connecting different single-wall carbon nanotubes (SWCN) to form three-terminal nanotube heterojunctions have been proposed recently.[6–9] In particular, we suggested the use of carbon nanotube ''T'' and ''Y junctions'' as three-terminal nanoscale molecular electronic devices.[8,9]

Earlier experimental observations of carbon nanotube Y junctions[10,11] did not attract much attention for electronics applications due mainly to the difficulties associated with their synthesis and the complexities of their structures. In order for the Y junctions to be useful from device perspective, controlled and high-yield production of these junctions is required. Very recently, experimentalists have succeeded in developing template-based chemical vapor deposition,[12] and pyrolysis of organometallic precursor with nickelocene and thiophene techniques[13] that allows for the reproducible and high-yield fabrication of carbon nanotube Y junctions.[12,13] While the template-produced junctions consisted of large diameter stems with two smaller branches with an acute angle between them resembling ''tuning forks,''[12] the pyrolysis method produced multiple Y junctions along a continuous nanotube.[13] The conductance measurements on these Y junctions have shown intrinsic nonlinear and asymmetric *I-V* behavior at room temperature.[13,14]

Following the experimental works reporting the controlled and high-yield synthesis of carbon nanotube Y junctions, we calculated the current vs voltage (*I-V*) characteristics of these junctions. In order to make a direct comparison with experiments, our work mainly focused on semiconducting Y junctions with symmetric branchings. Our results showed rectification for these junctions supporting the experimental findings. The highlights of our paper have recently been published in short articles.[15,16] In this paper, we present a detailed study of *I-V* characteristics of Y junctions with various combinations of stem and branch diameters and chiralities.

This paper is organized as follows: In Sec. II, we describe the relationship between the number of defect rings and the number of branches for an arbitrary nanotube junction. In Sec. III, we detail the formalism for calculating quantum conductivity of three-terminal junctions. In Sec. IV, we discuss the ballistic switching applications of SWCN Y junctions. Our results are presented in Sec. V. A discussion of our results is in Sec. VI.

II. TOPOLOGICAL CONSIDERATIONS

Although pristine SWCNs contain only hexagonal arrangement of carbon atoms, formation of a multiterminal junction requires the presence of topological defects in the form of pentagons, heptagons, and octagons. This is essential for maintaining sp^2 configuration for all carbon atoms in order to maximize stability. It is interesting to note that topological defects in multiterminal junctions including the Y junctions obey a generalization of the well-known Euler's formula. By considering only nonhexagonal polygons on the surface of a closed polyhedron in terms of the faces, vertices, and edges, a consideration for the formation of complex multiple junctions in terms of local bond surplus at the junction was proposed by Crespi.[17] The excess in the number of po-

lygonal sides due to nonhexagonal polygons is called local bond surplus. For example, the presence of a pentagon in an otherwise hexagonal sheet contributes to a bond surplus of -1, while heptagons and octagons contribute to bond surpluses of $+1$ and $+2$ each, respectively. The consideration proposed by Crespi is that a junction or a series of junctions made of N half nanotubes have a bond deficit of $6(N-2)$. For all three-point junctions (such as Y junctions) this gives a bond surplus of $+6$, and for all four-point junctions this gives a bond surplus of $+12$ at the junctions. In the Appendix we show the equivalence of Crespi's consideration with Euler's rule.

III. QUANTUM CONDUCTANCE OF SWCN THREE-TERMINAL JUNCTIONS

In this section, we present details of an embedding Green's-function approach for the calculation of quantum conductivity of three-terminal SWCN junctions. The formalism for simple two-terminal junctions have been detailed elsewhere.[18]

The most commonly used computational schemes for calculating the (coherent) current-voltage, $(I\text{-}V)$, characteristics of single-wall carbon nanotubes (SWCN) in contact with metal leads is based on the Landauer expression[19] which relates the electron conductance, G, with the transmission function, $T(E)$ (for a recent review see Ref. 20). The latter is usually obtained within either the transfer Hamiltonian approach[21,22] or the Green's-function scattering formalism.

The Green's function scattering approach is based on the existing relationship between the Green's function and the transmission function.[23,24] This approach appears to be equivalent to the weak-coupling version of Bardeen's transfer Hamiltonian[21] as discussed by Datta[25] (provided that one of the metal-tube couplings is weak).[26] The Green's-function approach coupled with a simple tight-binding model with one π electron per atom has been used by many groups to calculate the SWCN conductivity.[28,27]

Use of the Green's functions also allows us to utilize various embedding schemes that have been used with success in electronic structure calculations.[29–35] Recently, using the Green's function approach in conjunction with the embedding scheme of Inglesfield and Fisher,[32,35] we proposed an efficient computational scheme[18] that was used to obtain the $I\text{-}V$ characteristics of two-point (straight) SWCN junction in contact with metal leads. The extension of this formalism to three-point junctions (detailed next) was used to calculate the $I\text{-}V$ characteristics of SWCN Y junctions.[15,16]

A. Calculation of the *I-V* characteristics

We make the assumption that each of the N metal-leads $M_j(hkl)$, $(j=1,\ldots,N)$ is oriented in such a way that the $\langle hkl\rangle$ planes of the host lattice (metal lead) is parallel to the tube-lead interface and taken to be semi infinite. When the system is subjected to a bias voltage, V_j, the effect of the metal lead can be described entirely by introducing a self-energy term $\Sigma_j(E;V_j)$ which acts on the tube atoms in contact with this lead. As a result, the tube Hamiltonian H of a tube in contact with N-metal leads takes the form[24]

$$H=H(E;\mathbf{V})=H_C-\sum_{j=1}^{N}\Sigma_j(E;V_j), \tag{1}$$

where H_C is the Hamiltonian of the free tube and the symbol $\mathbf{V}$ is used to represent the set of bias-voltages V_j ,$j=1,\ldots,N$ applied to the N metal leads, respectively.

The Hamiltonian H contains most of the information about the tube in contact with the metal leads; its solution provides all the necessary factors for calculating specific properties of interest. In the present paper, we proceed by calculating the Green's function G_C associated with the Hamiltonian of Eq. (1), by a simple inversion, i.e.,

$$G_C(E;\mathbf{V})=\left(E-H_C-\sum_{j=1}^{N}\Sigma_j(E;V_j)\right)^{-1}. \tag{2}$$

In the tight-binding formulation used in the present paper both the Hamiltonians and the Green's functions are each taken to be $N_{at}N_{orb}\times N_{at}N_{orb}$ matrices, where N_{at} is the number of atoms in the embedding subspace and N_{orb} is the number of orbitals on each atom. We use $N_{orb}=4$ for carbon that includes $1-s$ and $3-p$ orbitals. Additionally, we use $N_{orb}=9$ for Ni (taken to be the material of the leads) that includes $1-s$, $3-p$, and $5-d$ orbitals. The metal lead is taken to be a $3d$ transition metal. We note that with some exceptions (see Refs. 27,36,38) most of the previous works on quantum transport of relatively large systems use only one π-electron orbital per atom.

In terms of the Green's function [given by Eq. (2)], the transmission function $T_{ij}(E;\mathbf{V})$ between the ith and jth metal leads kept at the bias voltages V_i and V_j, respectively, is obtained from the following equation:[24]

$$T_{ij}(E;\mathbf{V})=\mathrm{tr}[\Gamma_i(E;V_i)G_C(E;\mathbf{V})\Gamma_j(E;V_j)G_C^{\dagger}(E;\mathbf{V})],$$
$$i,j=1,\ldots,N, \tag{3}$$

where

$$\Gamma_j(E;V_j)=i[\Sigma_j(E;V_j)-\Sigma_j^{\dagger}(E;V_j)],j=1,\ldots,N. \tag{4}$$

Having obtained the functions T_{ij} $(E;\mathbf{V})$, we next use the formalism of Landauer, Datta, and Buttiker[19,24,37] to calculate the current I_i passing through the branch i of the tube for $i=1,\ldots,N$ in terms of the applied branch voltages V_i,$i=1,\ldots,N$, according to the expression

$$I_i=\frac{2e}{h}\sum_{j=1}^{N}\int_{-\infty}^{+\infty}dE\,T_{ij}(E;\mathbf{V})[f(\mu_i)-f(\mu_j)], \tag{5}$$

where f is the Fermi function, E_F the Fermi energy of the system and, $\mu_i=E_F-eV_i$. f is expressed in terms of the temperature T and Boltzmann's constant k_B in the usual way,

$$f(\mu_i)=1/[1+\exp(E-\mu_i)/k_BT]. \tag{6}$$

B. Evaluation of self-energy terms

The main computational step in calculating the $I\text{-}V$ characteristic of a SWCN (straight or multiterminal) is the calcu-

lation of the self-energy terms $\Sigma_j(E;V_j)$, $j=1,\ldots,N$ which describe the interaction between the jth metal lead with the jth branch of the SWCN, $j=1,\ldots,N$. We accomplish this by utilizing the embedding scheme of Inglesfield and Fisher.[32,35] This method is an alternative application of the Green's-function matching method that has been used in different forms recently in various studies.[27,29–31,38] We demonstrate our approach by applying to a simpler system consisting of a semi-infinite SWCN in contact with a semi-infinite metal lead: i.e., a semi-infinite SWCN connected at one of its ends to a semi-infinite metallic lead. Within an embedding scheme, the metallic lead (say the jth one) takes the place of a host lattice in which the nanotube is assumed to be embedded. We then construct a boundary surface $\mathbf{S}_j$ which separates the embedded system (tube) from the host lattice (lead). According to Inglesfield's approach,[32] (see also Ref. 34), the effect of the host lattice can be efficiently incorporated into the bare tube Hamiltonian through a surface inverse of the Green's function of the free host crystal obeying Neumann's boundary condition on $\mathbf{S}_j$. As shown by Fisher,[35] the process of the surface-inversion can be avoided if the Green's function of the free substrate satisfies the Dirichlet's condition on the boundary surface $\mathbf{S}_j$. According to Fisher,[35] if $G(\mathbf{r}_1,\mathbf{r}_2;E)$ is the Green's function of the host satisfying the Dirichlet's boundary condition on $\mathbf{S}_j$, then the host-tube interaction, $\Sigma_{S_j}(\mathbf{r}_1,\mathbf{r}_2;E)$, ($\mathbf{r}_1,\mathbf{r}_2$, defined on $\mathbf{S}_j$), can be evaluated from the following formula:

$$\Sigma_{S_j}(\mathbf{r}_1,\mathbf{r}_2;E)=-\frac{1}{4}\frac{\partial^2}{\partial n_1^{(j)}\partial n_2^{(j)}}G^{(j)}(\mathbf{r}_1,\mathbf{r}_2;E) \qquad (7)$$

where $\partial/\partial n^{(j)}$ denotes the derivative normal to $\mathbf{S}_j$.

Here, $\Sigma_{S_j}(\mathbf{r}_1,\mathbf{r}_2;E)$ [to be denoted simply by $\Sigma_j(\mathbf{r}_1,\mathbf{r}_2;E)$ in the following] is the electron self-energy (SE) term that describes the interaction of the jth metal lead with the tube if $G^{(j)}(\mathbf{r},\mathbf{r}';E)$ is taken to be the Green's function for the unperturbed jth metal lead. The problem of constructing the lead-tube interaction, therefore, becomes a problem of constructing the Green function of a semi-infinite metal lead satisfying the Dirichlet's condition on the lead-tube interface. For this step, we follow the method of Sanvito *et al.*[39] This state-of-the-art embedding scheme, thus, allows a realistic description of the lead-metal interaction.

It is worth noting that the present approach is similar in spirit to the subspace Hamiltonian method that we have used in earlier studies[29–31] and with that of Nardelli as well as that of Nardelli and Bernholc.[27,38] The unique feature in the present approach, however, is that the effect of the metal leads on the SWCN is entirely described by quantities of the host material solely. This is a basic feature of the embedding scheme of Inglesfield.[32] (See also the work of Baraff and Schluter[33] for further details).

In order to utilize the Inglesfield-Fisher[32,35] embedding approach to calculate the tube-lead interaction in the case of a multiterminal SWCN of finite length with N branches connected to N metal leads, we take each metal lead as a semi-infinite metal and proceed with the calculation of each self-energy $\Sigma_j(E;V_j)$, $j=1,\ldots,N$, in the same way as described in the case of semi-infinite SWCN in contact with a semi-infinite metal lead. The Green's function G_C of the combined tube-leads system and the transmission functions, $T_{ij}(E;\mathbf{V})$, are then obtained using Datta's formulation[24] according to Eqs. (1)–(4).

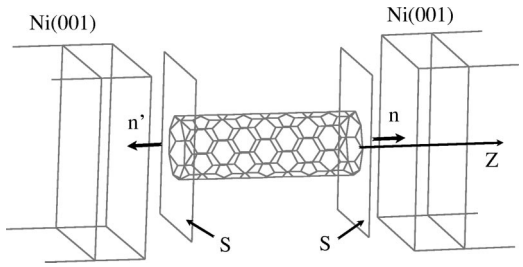

FIG. 1. Schematic representation of the basic geometry of the system considered in the present paper consisting of a straight SWCN connected to metal leads.

Figure 1 shows the basic geometry of the system considered in the present paper consisting of a straight SWCN connected to metal leads. The metal lead is assumed to be oriented in such a way that the (hkl) planes of the host lattice (metal lead) is parallel to the tube-lead interface.

The plane passing through the carbon atoms forming the ring at the far end of the jth stem of the SWCN is taken to be parallel to the (hkl) lattice planes of the semi-infinite jth metal lead. Furthermore, the carbon ring is located at a distance equal to the interplanar distance of the (hkl) lattice planes in the bulk phase of the metal lead. The plane of the jth metal lead in contact with the carbon ring of the jth branch of the SWCN is taken to be the $\mathbf{S}_j$ surface on which the Green's function of the left metal lead satisfies the Dirichlet's boundary condition.

C. Evaluation of Green's function of metal-lead

In the case where the metal lead is taken to be a semi-infinite periodic system, one can proceed with the construction of the Green's function of the metal lead by following the work of Sanvito *et al.*[39] In a matrix formulation of their theory, the Green's function of the metal lead, which satisfies Dirichlet's boundary condition on $\mathbf{S}_j$ (taken to be the $z=z_0$ plane) takes the form,

$$G^{latt}(z,z';E)=-2[\Phi\Lambda(z-z')\Phi^{\dagger}-\overline{\Phi}\,\overline{\Lambda}(z-z_0)\times\overline{\Phi}^{\dagger}\Phi\Lambda(z_0-z')\Phi^{\dagger}]\Pi^{-1}, \qquad (8)$$

$$\Pi=\Phi\kappa\Phi^{\dagger}-\overline{\Phi\kappa\Phi^{\dagger}}, \qquad (9)$$

where Φ, $(\overline{\Phi})$ is the matrix consisting of the set of eigenvectors of the tight-binding (TB) Hamiltonian propagating to the right (left) and decaying to the right (left).

The Hamiltonian of each metal-lead has the form

$$H_{latt}=\begin{pmatrix}-H_1^{-1}(H_0-E) & -H_1^{-1}H_1^{\dagger}\\ \mathbf{I} & \mathbf{0}\end{pmatrix}, \qquad (10)$$

where the matrices H_0, H_1, **I**, and **0** are $N\times N$ matrices ($N=N_{at}N_{orb}$) with **I**, **0** being the unit and null matrices, respectively. H_0 the intralayer and H_1 the interlayer Hamiltonians as defined by Sanvito *et. al.*[39] (The layer is taken to be a lattice plane parallel to the surface). Note that H_{latt} is complex and, in general, non-Hermitian. Two sets of eigenvectors, therefore, must exist representing ''left'' and ''right.'' In particular, eigenvectors Φ_j and $\overline{\Phi}_j$ are the upper half components of the corresponding ''left'' and ''right'' eigenvectors, respectively, of the matrix H_{latt}. The eigenvalues corresponding to the eigenvectors Φ_j ($\overline{\Phi}_j$) are written in the general complex form e^{ik_ja} ($e^{i\overline{k}_ja}$), a being the interplanar distance of the (hkl) lattice planes of the metal lead. The wave-vectors k_j ($\overline{k}_j$) are complex numbers in general. The matrices κ and $\Lambda(z)$ [and $\overline{\kappa}$ and $\overline{\Lambda}(z)$] are diagonal $N\times N$ matrices related by the equation,

$$\kappa=\frac{d}{dz}\Lambda(z) \tag{11}$$

with

$$\Lambda_{jj}(z)=e^{ik_jz}. \tag{12}$$

It is now straightforward to show that in this case, the SE [calculated according to Eq. (7)] takes the form (for $z=z'=z_0-\nu a$, where ν is a real number),

$$\Sigma_{S_j}(E)=-\frac{1}{2}[\Phi\kappa\lambda_\nu^{-1}\Phi^\dagger-\overline{\Phi\kappa\lambda_\nu^{-1}\Phi^\dagger}]\Phi\kappa\lambda_\nu\Phi^\dagger\Pi^{-1}, \tag{13}$$

where λ_ν is a diagonal $(N\times N)$ matrix with diagonal elements

$$(\lambda_\nu)_{jj}=e^{ik_j\nu a}. \tag{14}$$

For λ_ν equal to the unit matrix ($\nu=0$), Eq. (13) reduces to

$$\Sigma_{S_j}(E)=-\frac{1}{2}\Pi\Phi\kappa\Phi^\dagger\Pi^{-1}=-\frac{1}{2}\Phi\kappa\Phi^\dagger. \tag{15}$$

In this form, its relationship to the corresponding result derived for the jellium case should be apparent.[18] The present paper requires that we take $\nu=0$.

D. Brief review of tight binding molecular-dynamics method and approximations used

One of our approximations has to do with the fact that while the SEs constructed are expressed in the basis-set representation of atomic orbitals centered on the lattice points of the metal leads, the basis set used for the TB representation of the bare tube is based on atomic orbitals centered on the tube atoms. As the tube atoms affected by the contacts are not always located on lattice points of the metal leads, it becomes necessary to transform the TB description of the SE from one representation to the other. Within our tight binding molecular-dynamics (TBMD) approach, because we are using universal TB parameters,[40] the simplest way to achieve this is to take the same number of orbitals for the tube as well as the metal-lead atoms and assume that the TB parameters of the SEs can be scaled with respect to the inter-atomic distance according to the same law as the TB parameters of the SWCN (see, for example, Ref. 41). Another approach would be to take the metal-lead atoms, which are in direct contact with the tube, as part of the tube and apply the SEs on these metal-lead atoms. In the latter case, however, a broadening of the resonance peaks of the transmission functions $T_{ij}(E;\mathbf{V})$ is expected.[42] In the present paper, we take the same number of basis functions to describe both the metal and the SWCN but avoid any scaling corrections for simplicity. Thus, our method is not restricted to idealized surfaces as shown in Fig. 1. Instead, by considering the lead atoms of the contact regions as part of the tube (with tube atoms relaxed) we are able to study the effect of the microscopic contact details on the transport properties of the SWCNs. Full consideration of the lead-nanotube interface that includes the relaxation of lead atoms is a computationally intensive endeavor and outside the scope of the present paper. Nevertheless, our calculations on smaller two-probe (straight) SWCNs have shown (in agreement with Ref. 41) that the inclusion of the metal lead atoms in the tube Hamiltonian does not change the qualitative features of the I-V curves; their main effect being the broadening of the resonance peaks of $T(E)$. Therefore, in the present paper, we used the approximation of Eq. (16) in the calculations that follow.

Another approximation pertains to the effect of the applied bias voltages, $V_j, j=1,\ldots,N$, on the transmission functions $T_{ij}(E;\mathbf{V})$ and the self-consistency requirements. This is because the bias voltages shift the Fermi level of each metal lead relative to that of the bare tube and, this in turn, gives rise to charge transfer from the metal leads towards the tube atoms or vice versa. The charge-transfer process tends to smooth out the abrupt potential step introduced by the bias voltage at the metal-tube interface. As Farajian *et. al.* have shown,[43] this smoothing effect is more pronounced at high bias voltages and exhibits Friedel-type oscillations which decay quickly away from the interface. Although we have developed a self-consistent tight binding molecular-dynamics (TBMD) formalism[44] capable of treating charge-transfer effects effectively, we have found it computationally prohibitive to include charge transfer in our studies of the transport properties of the SWCNs. For this reason and due to the fact that the smoothing effect due to charge transfer is quite small for low bias voltages,[43] we have ignored the smoothing process and focused only on the effect of the bias voltage on the transmission function of a straight SWCN.[18] We have shown that when the applied bias voltage is symmetrically distributed between the two metal leads (i.e., adopting the $\eta=1/2$ model of Tian *et al.*[45]), the approximation

$$T_{ij}(E;\mathbf{V})\approx T_{ij}(E) \tag{16}$$

is very satisfactory as expected.[46] We have tested the approximation dictated by Eq. (16) in the case of Y-junction SWCNs (YSWCNs) when biased according to Eq. (17) (shown below). It was found that using the exact voltage dependence of $T_{ij}(E;\mathbf{V})$ the calculated I-V characteristics do

not differ appreciably from those obtained using the approximation dictated by Eq. (16). Thus, in the present paper we used the approximation of Eq. (16) in the calculations that follow.

IV. BALLISTIC SWITCHING AND RECTIFICATION

Soon after their production, it was experimentally confirmed that YSWCNs exhibit rectification properties.[12,14] At the same time, theoretical investigations predicted the possibility of YSWCNs to operate as ballistic switches in a way analogous to that observed in Y-branch switches, (YBSs), made from materials other than carbon nanotubes, as for example in YBSs based on the $InP/In_xGa_{x-1}As$ heterojunctions.[47]

The experimental setups used for studying the rectification and switching properties of YSWCNs and/or YBSs consist of[12,14,47] (in the following we will use the terms *left branch*, to be labeled by *L*, and *right branch*, to be labeled by *R*, to denote the two branches of the YSWCN and will use the term *stem*, to be labeled by *S*, to denote the remaining third branch)

(1) Setup for determining the *I-V* characteristics. Both the left and right branches are grounded and the stem is biased at the bias voltage V_b, i.e.,

$$V_L = V_R = 0.00; \quad V_S = V_b. \tag{17}$$

In this setup one measures the dependence of the currents I_L, I_R, and I_S on the bias voltage V_b.

(2) Switching Setup-1. The stem is grounded while the left and right branches are biased as follows:

$$V_L = -V_R = V_b; \quad V_S = 0.00. \tag{18}$$

In this setup, one measures the dependence of the stem current I_S on the bias voltage V_b under the condition $V_S = 0.00$.

(3) Switching Setup-2. The stem is biased at voltage V_S while the right and left branches are biased as follows:

$$V_L = -V_R = V_b; I_S = 0.00. \tag{19}$$

This setup, while experimentally feasible for YBSs, is currently not feasible for YSWCNs. In this setup, one measures the dependence of the stem voltage V_S on the bias voltage V_b under the condition $I_S = 0.00$.

In the next section, we will present theoretical results for the *I-V* characteristics and the dependences $I_S = f(V_L = -V_R)|_{V_S=0}$ and $V_S = f(V_L = -V_R)|_{I_S=0}$ for YSWCNs consisting of SWCNs of different chiralities, both metallic and semiconducting.

V. RESULTS

In this section we present our results of quantum conductivity calculations for various SWCN Y junctions. Since the Y junctions are formed by the joining of three SWCNs, diameter and chirality considerations lead to a large number of possible permutations. The calculations of the *I-V* characteristics of all the possible Y junctions are, therefore, clearly not feasible. In order to make the problem tractable, we divide the Y junctions into two main categories and perform quantum conductivity calculations on a few Y junctions belonging to each category. As will be seen later, many interesting patterns can be deduced by a study of these junctions. The two categories consist of; (a) no change in chirality on branching and (b) change in chirality on branching.

All these structures are relaxed using the nonorthogonal TBMD of Menon and Subbaswamy.[48,49] In all cases studied, we used metal leads made of semi-infinite Ni metal in the $\langle 001 \rangle$ orientation. I.e., we have taken the $\langle 001 \rangle$ lattice plane of the semi-infinite Ni to be the contact plane at each metal-tube contact with the metal plane positioned at a distance equal to the bulk-$\langle 001 \rangle$-interplanar distance from the outermost carbon ring of the corresponding YSWCN stem. In this way, the transport properties that are computed in the present paper for the various tubes correspond to the same contact and bias configurations, a condition that is necessary for a meaningful comparison of the obtained results.

The TB formalism used is the same as that used previously to treat Ni-C systems.[41] This method has been used with success in the treatment of interactions of Ni with graphite,[41] C_{60},[50,51] SWCNs,[52–54] as well as benzene molecules.[55]

A. Y junctions with no change in chirality on branching

The four different Y junctions with all zigzag arms are shown in Fig. 2. They consist of (a) a (14,0) stem branching into two (7,0) tubes, (b) three (8,0) branches, (c) a (17,0) stem branching into (10,0) and (7,0) tubes with an acute angle between them and, (d) another (17,0) stem branching into (10,0) and (7,0) tubes, but with a different angle between the branches than in (c). The branching is symmetric in (a) and (b) and asymmetric in (c) and (d). The defect rings are shown in dark. In Fig. 2(a) *S*,*L*, and *R* denote stem, left, and right branches, respectively, of the Y junction. All these Y junctions are semiconducting.

Note that each of these Y junctions satisfy the criteria for multiterminal junctions described in Sec. II with a bond surplus of +6. In the Y junctions shown in Fig. 2 the structures (a), (b), and (c) contain six heptagonal defects each, while the structure in (d) contains four heptagons and an octagon.

Figure 3 shows the *I-V* characteristics of the (14,0)-(7,0)-(7,0) Y junction [Fig. 2(a)] biased according to Eq. (17). The current direction is taken to be positive when flowing towards the junction region and negative otherwise. As seen in the figure, there is perfect rectification, i.e., current is nonzero only when the bias voltage is negative. In the top inset we show the dependence $I_S = f(V_b)|_{V_S=0}$ under the biasing conditions given by Eq. (18). The symmetry in the currents is evident in the figure indicating perfect switching. As can be seen in the figure, I_S is always positive regardless of whether the biasing is from the left or right branches. Further insights into the switching properties can be gained by studying the $V_S = f(V_b)$ dependence given by the biasing condition in Eq. (19). The results are shown in the bottom inset. The para-

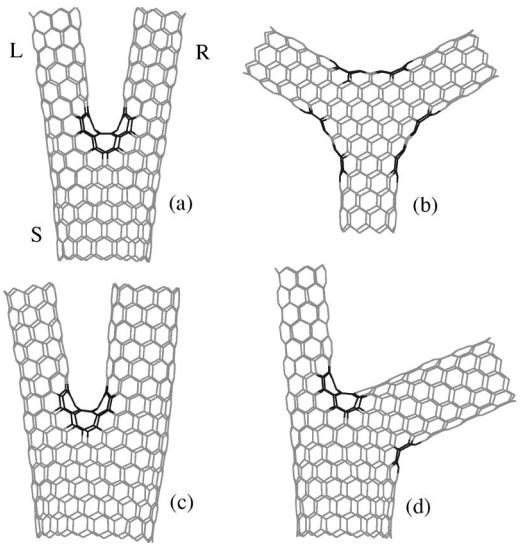

FIG. 2. The four different Y junctions made up of all zigzag arms. They consist of; (a) (14,0) stem branching into two (7,0) tubes symmetrically, (b) three (8,0) branches, (c) a (17,0) stem branching into (10,0) and (7,0) tubes with an acute angle between them and, (d) another (17,0) stem branching into (10,0) and (7,0) tubes, but with a different angle between the branches than in (c). In (a), *S*,*L* and *R* denote stem, left, and right branches, respectively of the Y junction. The atoms forming the defect rings are shown in dark.

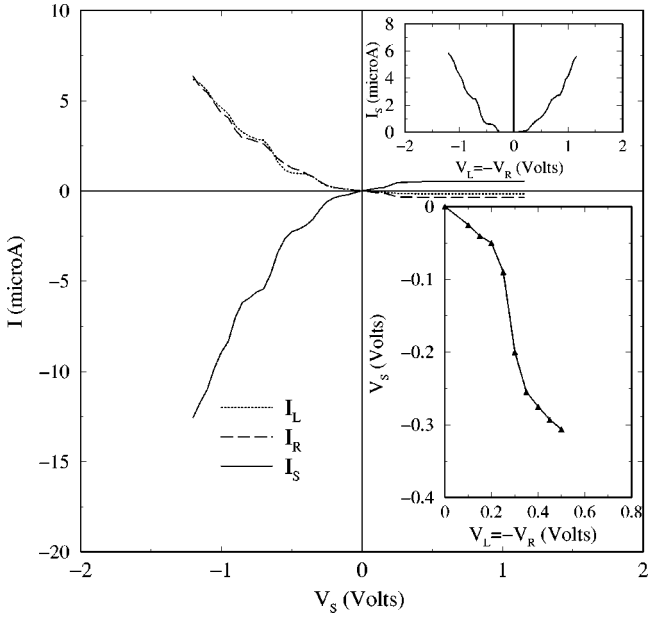

FIG. 3. The I-V characteristics of the (14,0)-(7,0)-(7,0) symmetric Y junction [Fig. 2(a)] biased according to Eq. (17) showing rectification. The current direction is taken to be positive when flowing towards the junction region and negative otherwise. The top inset shows $I_S = f(V_b)|_{V_S=0}$ dependence under the biasing conditions given by Eq. (18). The symmetry in the currents indicates perfect switching. The bottom inset shows $V_S = f(V_b)|_{I_S=0}$ dependence given by the biasing condition in Eq. (19).

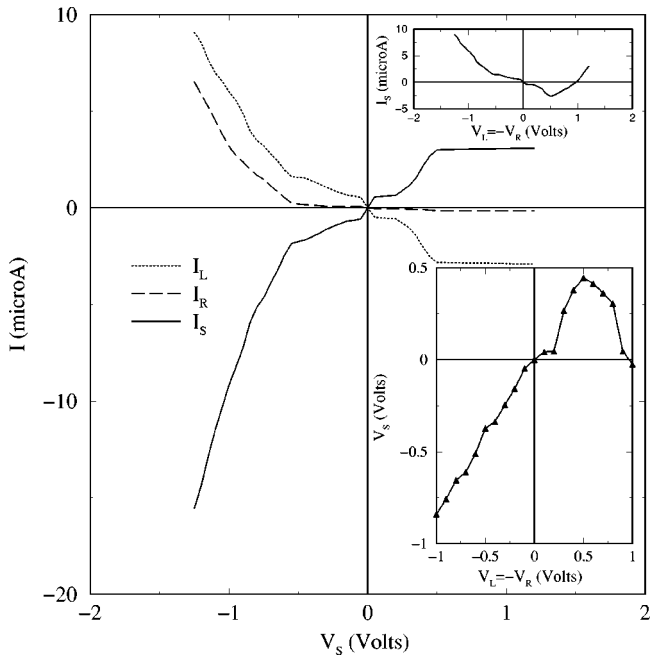

FIG. 4. The *I*-*V* characteristics of the (17,0)-(10,0)-(7,0) asymmetric Y junction [Fig. 2(c)] biased according to Eq. (17) showing the absence of rectification. The top inset shows the $I_S = f(V_b)|_{V_S=0}$ dependence under the biasing conditions given by Eq. (18) showing asymmetry in the currents and the loss of the perfect switching feature. The bottom inset shows the $V_S = f(V_b)|_{I_S=0}$ dependence.

bolic dependence of V_S on V_b seen is very similar to that observed in the case of Y-branch switches (YBS)[56] made from materials other than carbon nanotubes, as for example in YBSs based on the $InP/In_xGa_{x-1}As$ heterojunctions.[47]

The *I*-*V* characteristics of the (17,0)-(10,0)-(7,0) Y junction [Fig. 2(c)] biased according to Eq. (17) is shown in Fig. 4. As seen in the figure, there is no rectification for this asymmetric Y junction. The top inset shows the $I_S = f(V_b)|_{V_S=0}$ dependence under the biasing conditions given by Eq. (18). Although, the arrangement of defects is identical to that in Fig. 2(a), there is asymmetry in the currents and the loss of the perfect switching feature. The $V_S = f(V_b)$ dependence [biased according to Eq. (19)] of this Y junction is shown in the bottom inset. As seen in the figure $V_S(-V_b) \neq V_S(V_b)$ and there is no overall parabolic dependence.

We also note that results of the conductance calculations for the (8,0)-(8,0)-(8,0) Y junction [Fig. 2(b)] were very similar to those obtained for the (14,0)-(7,0)-(7,0) Y junction [Fig. 2(a)], i.e., rectification and perfect switching. Not surprisingly, results for the Y junction in Fig. 2(d) were very similar to those obtained for the Y junction in Fig. 2(c).

We have also calculated the *I*-*V* characteristics of a (14,0)-(10,0)-(7,0) Y junction. This junction, although asymmetric, shows perfect rectification despite not exhibiting switching properties.

We next study Y junctions with stem and branches consisting of ''armchair'' nanotubes. In Fig. 5 we show two such Y junctions. They consist of (a) (10,10)-(5,5)-(5,5) and (b) (10,10)-(5,5)-(4,4) Y junctions. They each contain topologi-

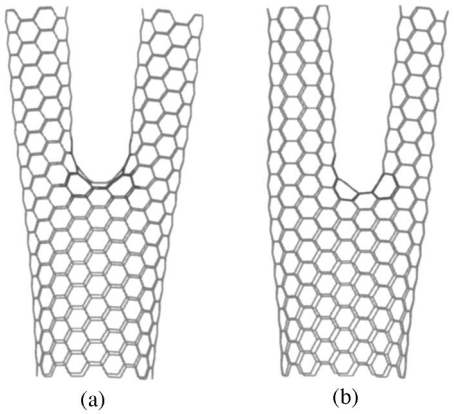

FIG. 5. Y junctions with stem and branches consisting of ''arm-chair'' nanotubes. They are; (a) (10,10)-(5,5)-(5,5) and, (b) (10,10)-(5,5)-(4,4) Y junctions.

cal defects in the form of six heptagons. The *I-V* characteristics of the symmetric (10,10)-(5,5)-(5,5) and asymmetric (10,10)-(5,5)-(4,4) Y junctions are shown in Figs. 6 and 7, respectively. In each of these cases there is asymmetry with some leakage currents for positive bias voltages. The top insets contain $I_S = f(V_b)|_{V_S=0}$ dependence under the biasing conditions given by Eq. (18) and show negative resistance and lack of perfect switching. The bottom insets show $V_S = f(V_b)$ dependence indicating lack of perfect switching. The insets also show the manifestation of topological asymmetry in the case of the (10,10)-(5,5)-(4,4) Y junction. We have also considered a (10,10)-(3,3)-(3,3) Y junction. The results obtained were similar to the (10,10)-(5,5)-(5,5) case.

B. Y junctions with change in chirality on branching

In Fig. 8 we show four different Y junctions. They consist of (a) (10,10)-(8,0)-(8,0), (b) (10,10)-(9,0)-(9,0), (c) (14,0)-(4,4)-(4,4), and (d) (18,0)-(4,4)-(4,4) Y junctions. In each of these Y junctions, the chirality of the branches differ from that of their stems. In (a) the metallic armchair nanotube branches into two semiconducting zigzag nanotubes. The *I-V* characteristics are shown in Fig. 9 and shows asymmetric *I-V* characteristics with some leakage currents for positive bias voltages. The top inset contains $I_S = f(V_b)|_{V_S=0}$ dependence under the biasing conditions given by Eq. (18) and shows negative resistance and lack of perfect switching. The absence of perfect switching is further evident in the $V_S = f(V_b)$ dependence shown in the bottom inset.

The *I-V* characteristics of the structure in Fig. 8(b) in which a (10,10) metallic nanotube branches into two metallic zigzag (9,0) nanotubes is shown in Fig. 10. As seen in the figure, there is asymmetry with some leakage currents for positive bias voltages. The top inset contains $I_S = f(V_b)|_{V_S=0}$ dependence and shows perfect switching and no negative resistance. The perfect switching is also evident in the $V_S = f(V_b)$ dependence shown in the bottom inset.

The (14,0)-(4,4)-(4,4) Y junction [Fig. 8(c)] constitutes a semiconducting zigzag nanotube branching into two metallic arm-chair nanotubes. The *I-V* characteristics of this Y junction is given in Fig. 11 and shows perfect rectification.

The (18,0)-(4,4)-(4,4) Y junction [Fig. 8(d)], on the other hand, constitutes a metallic zigzag nanotube branching into two metallic arm-chair nanotubes. The *I-V* characteristics of this Y junction is given in Fig. 12 and also shows perfect rectification.

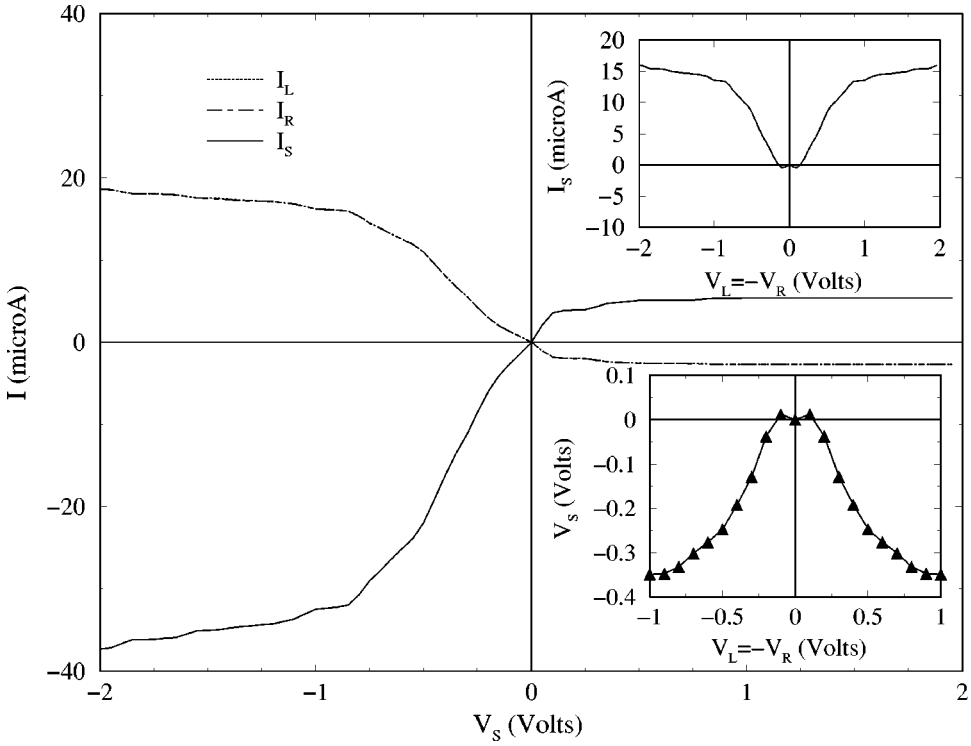

FIG. 6. The I-V characteristics of the symmetric (10,10)-(5,5)-(5,5) Y junction [Fig. 5(a)] showing asymmetry with some leakage currents for positive bias voltages. The top and bottom insets contain $I_S = f(V_b)|_{V_S=0}$ and $V_S = f(V_b)|_{I_S=0}$ dependences, respectively.

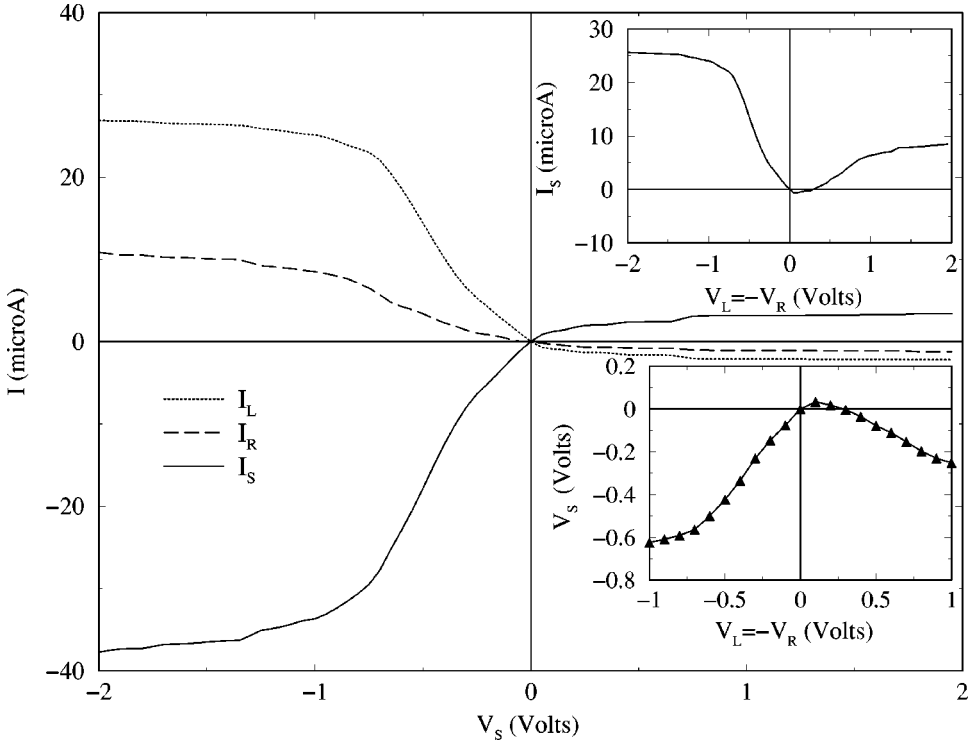

FIG. 7. The *I-V* characteristics of the asymmetric (10,10)-(5,5)-(4,4) Y junction [Fig. 5(b)] also showing asymmetry with some leakage currents for positive bias voltages.

A careful review of these results suggest the following:

(i) Perfect rectification is obtained for symmetric carbon nanotube Y junctions consisting of zigzag stems. These junctions also exhibit perfect switching features.

(ii) Asymmetric Y junctions show no rectification and do not exhibit switching properties; an exception being the (14,0)-(10,0)-(7,0) Y junction. It is worth noting that the angle between the branches here is close to 90^o.

(iii) Y junctions containing arm-chair stems, although showing asymmetric *I-V* characteristics, exhibit small leakage currents for positive bias voltages (''imperfect rectification''). This feature is found to be independent of the chirality and symmetry of the branches.

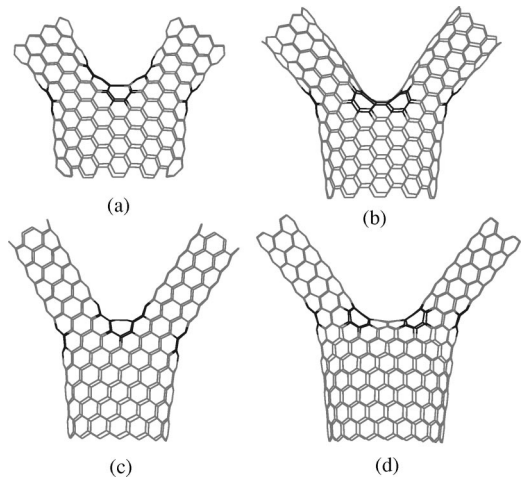

FIG. 8. Four Y junctions consisting of (a) (10,10)-(8,0)-(8,0), (b) (10,10)-(9,0)-(9,0), (c) (14,0)-(4,4)-(4,4), and (d) (18,0)-(4,4)-(4,4) Y junctions. The atoms forming defect rings are shown in dark. In each of these Y junctions, the chirality of the branches differ from that of their stems. The atoms forming the defect rings are shown in dark.

These observations and the fact that all tubes were studied under the same bias conditions lead to the conclusion that perfect rectification and switching properties are intrinsic properties of Y junctions exhibiting specific symmetry (D_{2v}) and consist of zigzag stems [i.e., $(n,0)$ type].

The D_{2v} symmetry of the tubes that we studied is reflected in the $V_S=f(V_L=-V_R=V_b)|_{I_S=0}$ and $I_S=f(V_L=-V_R=V_b)|_{V_S=0}$ dependences shown in the lower and upper insets of Figs. 3, 6, 9, 10, 11, and 12, respectively. These dependences were found to satisfy the following relations:

$$V_S(V_b)=V_S(-V_b), V_b=V_L=-V_R, \tag{20}$$

$$I_S(V_b)=I_S(-V_b), V_b=V_L=-V_R. \tag{21}$$

Small deviations observed in some cases are due to small deformations due to the dynamical relaxation process. Clearly, the relations (20) and (21) are not satisfied by the asymmetric tubes. It should be pointed out that the relation $V_S=V_S(V_b), V_b=V_L=-V_R$ is very sensitively dependent on the chirality of the branches and declines significantly from the parabolic dependence found in the Y branch switches.[47,57] In some cases, where a dip is observed in the variation of V_S as a function of $V_b=V_L=-V_R$, (in an otherwise monotonic behavior), it is observed that the corresponding variation $I_S(V_b)=I_S(-V_b)$, $V_b=V_L=-V_R$ exhibits regions of negative differential resistance (NDR). This appears very pronounced in the case of the (10,10)-(8,0)-(8,0) YSWCN and to a lesser extent in the (8,0)-(8,0)-(8,0) YSWCN. The technologically important properties exhibited

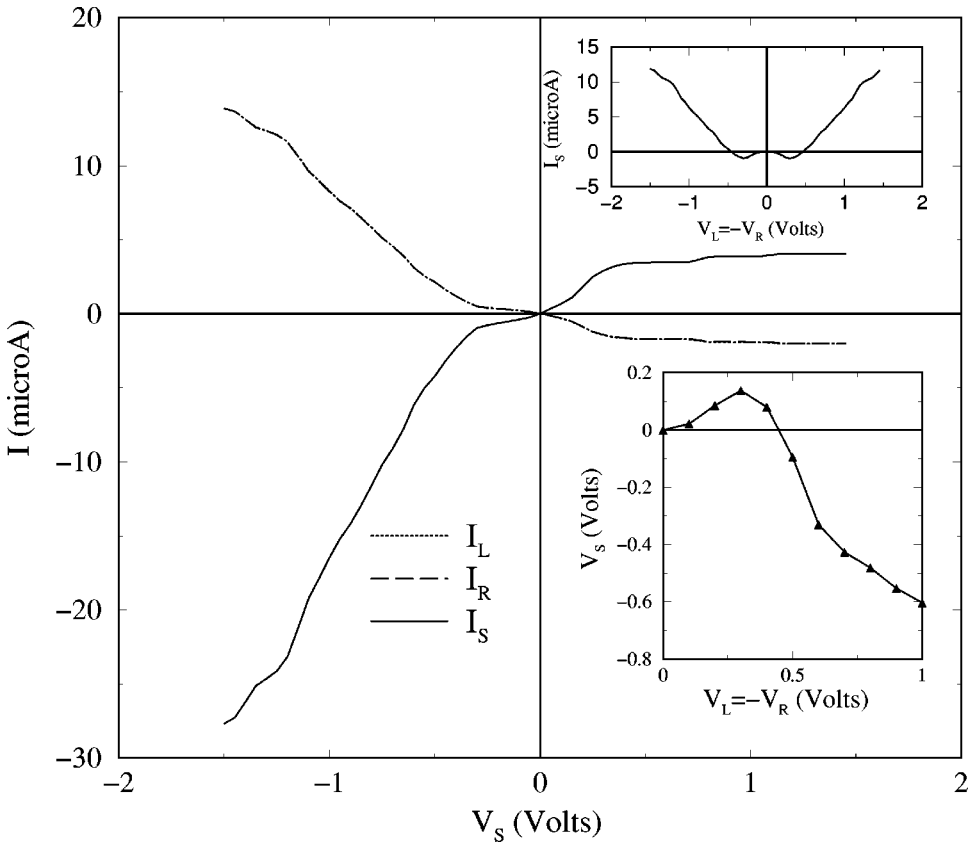

FIG. 9. The *I-V* characteristics for the (10,10)-(8,0)-(8,0) Y junction [Fig. 8(a)] showing asymmetry with some leakage currents. The top inset contains $I_S = f(V_b)|_{V_S=0}$ dependence under the biasing conditions given by Eq. (18) showing negative resistance and lack of perfect switching. The bottom inset contains $V_S = f(V_b)|_{I_S=0}$ dependence confirming lack of perfect switching.

such as rectification, switching, and the NDR make the YSWCN a very promising material in the emerging nanodevice industry.[56]

Similar rectification and/or switching properties were experimentally observed in Y-shaped branch switches (YBSs) of D_{2v} symmetry made of InP/$In_xGa_{x-1}As$ heterojunctions[47] and in the asymmetric microjunction studied by Song *et al.*[58,59] In the former case, the rectification and switching properties were attributed to features of ballistic transport inherently related to the InP/$In_xGa_{x-1}As$ heterojunctions. In the latter case, the rectification properties were attributed to dynamical nonlinear effects associated with the asymmetry of the microjunction. It should be noted, however, that the symmetric device studied by Song contained an asymmetric scatterer. Some other theoretical investigations on the rectification properties of YBSs attribute their properties on self-gating[56,60] and doping effects.[12,14] Our findings are more consistent with the theoretical conclusions arrived at by Treboux *et al.*[61] who found that symmetry-dependent interference effects can change the metallic character of zigzag YSWCNs to semiconducting.

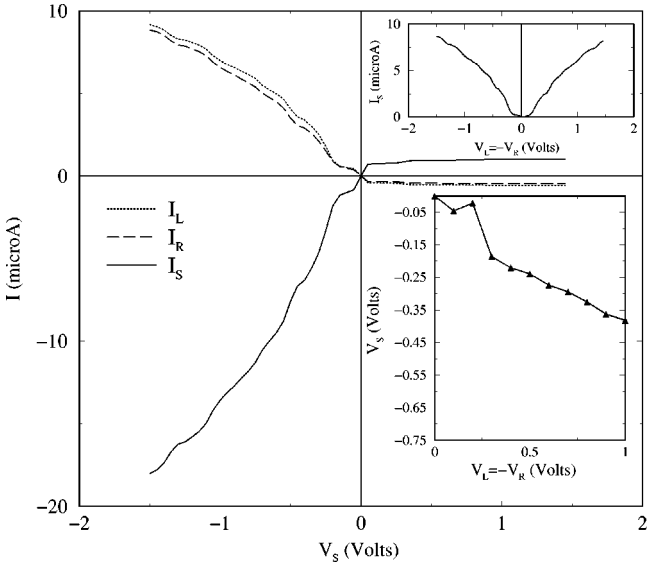

FIG. 10. The *I-V* characteristics for the (10,10)-(9,0)-(9,0) Y junction [Fig. 8(b)] showing asymmetry with some leakage currents. The top inset contains $I_S = f(V_b)|_{V_S=0}$ dependence under the biasing conditions given by Eq. (18) showing no negative resistance but perfect switching. The bottom inset contains $V_S = f(V_b)|_{I_S=0}$ dependence confirming perfect switching.

VI. DISCUSSION

The results presented in Sec. V seem to suggest that rectification observed in Y-junction nanotubes cannot be simply explained by chirality considerations alone and a number of other factors must be considered. We, therefore, invoke a model calculation to seek explanations for the rectification phenomena in carbon nanotube Y junctions.

Observing that interference is a general phenomenon in branched topologies, Treboux *et al.*[61] proceeded with one-dimensional-model (1D-model) calculations to demonstrate the effect of interference on the transmission properties of Y-shaped nanotubes. They have shown that main factors in-

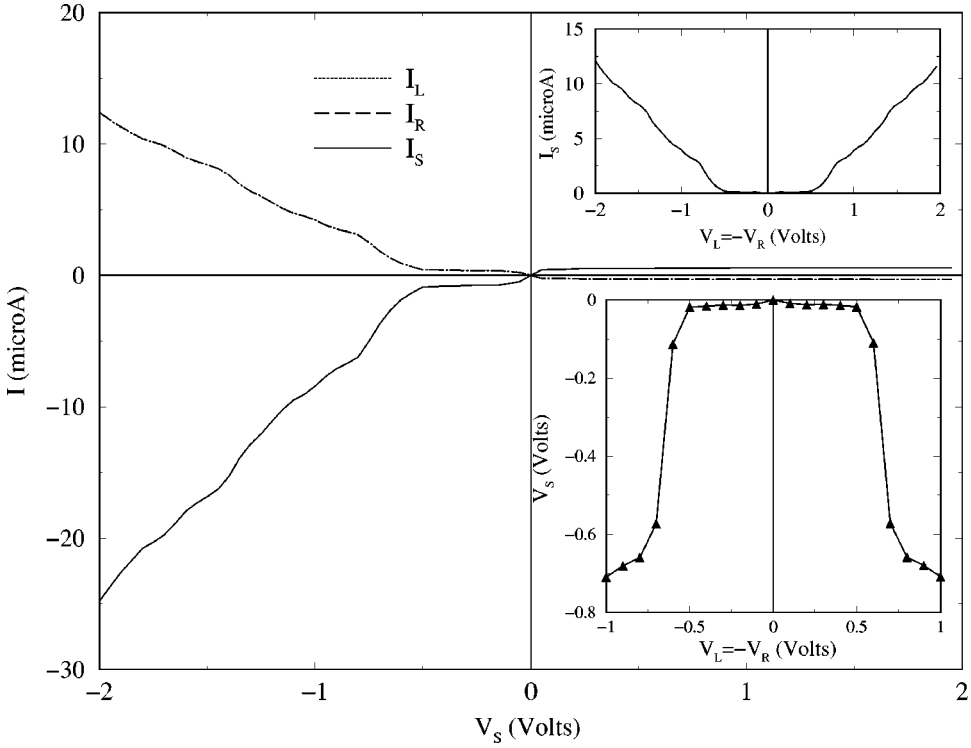

FIG. 11. The *I-V* characteristics for the (14,0)-(4,4)-(4,4) Y junction [Fig. 8(c)] showing perfect rectification.

fluencing the transmission function $T_{LR}(E)$ from the left (L) to the right (R) branch include; (i) the details (symmetry and geometry) of the Y junction (the ''spacer'' in Treboux's terms) and (ii) the length of the central (S) branch.

We perform, 1D-model calculations using similar reasoning as Treboux's *et al.* by considering the systems shown in Fig. 13. In this model system A [shown in Fig. 13(a)] consists of 60 atoms (20 in each branch) in a Y-shaped geometry in which the spacer consists of a single atom (to be termed spacer-A atom). In the same model, system B [shown in Fig. 13(b)] consists of 63 atoms (20 in each branch) in a Y-shaped geometry in which the spacer has the form of an hexagon, i.e., all of the atoms making up the hexagon are taken to be spacer atoms (to be termed spacer-B atoms). We denote the on-site energy of the spacer atoms by E_x and the on-site energy of all the other atoms (in all three branches) by E_0.

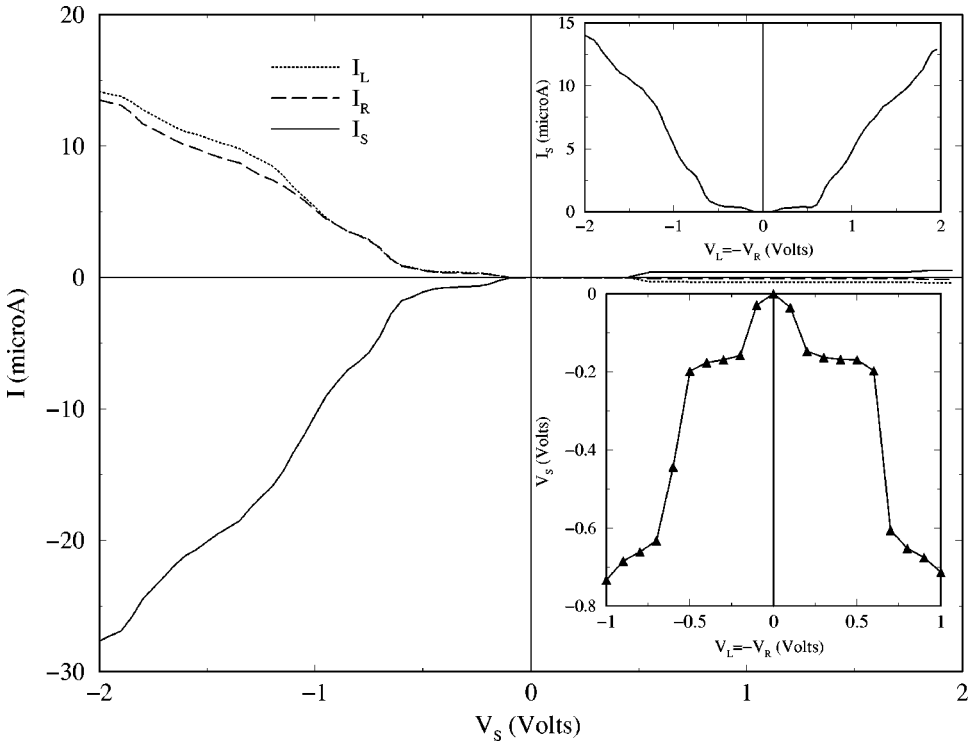

FIG. 12. The *I-V* characteristics for the (18,0)-(4,4)-(4,4) Y junction [Fig. 8(d)], also showing perfect rectification.

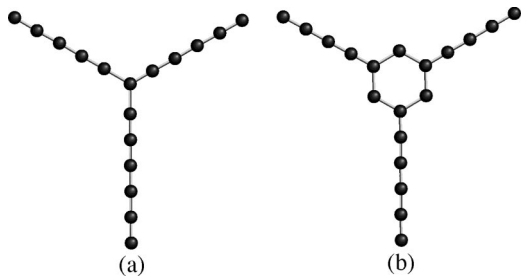

FIG. 13. Two 1D models used to explain rectification. (a) Model system A consisting of a Y-shaped geometry in which the spacer consists of a single atom and (b) model system B consisting also of a Y-shaped geometry in which the spacer has the form of an hexagon, i.e., all of the atoms making up the hexagon are taken to be spacer atoms.

Also, we denote by V_x the hopping integral between the spacer-A atom and its nearest neighbors (n.n) or the hopping integral between n.n spacer-B atoms. The hopping integral between all the other n.n. is denoted by V. For these two model systems we applied our formalism (described in Sec. III) for the calculation of the various components of the transmission function, $T_{ij}(E)$, $i,j=L,R,S$. The connection to the metal leads is described by a self energy term Σ_j,j $=L,R,S$ which is taken to be independent of the energy. Its actual value, within a reasonable range of values, was found not to affect the qualitative features of our results.

Our results for $T_{ij}(E)$, $i,j=L,R,S$ as a function of energy E, for different E_x and V_x values are shown in Figs. 14 and 15 corresponding to models A and B, respectively. In Fig. 14 corresponding to model A, we take $E_0=-5$ and the hopping integral not involving the spacer atoms, $V=-2.5$. As seen in the figure, $T_{LC}(E)=T_{RC}(E)\neq T_{RL}(E)$. This is because two of the branches behave essentially as chains of 21 atoms (including the spacer) while the third arm behaves as a 20-atom chain. In a 61-atom system the three transmission coefficients would have been identical for branches of equal length (see model B results below). Nevertheless, the system studied illustrates the effect of branch length on the transmission coefficients as shown by our model-A calculations. Figure 14(a) is analogous to that of Treboux *et al.* for the case of the semi-infinite S branch. The Y junction appears to allow transmission over the whole energy band. A noticeable difference, however, can be seen in our results as compared with those of Treboux *et al*. This is the oscillations that we find in the energy dependence of the $T(E)$'s. Another more interesting feature that emerges from our calculations is the dependence of $T(E)$'s on the on-site and hopping integrals of the spacer atoms. As can be seen in Fig. 14(b), the qualitative features of the transmission functions are not affected by a rather large variation in the on-site energy of the spacer atom. The situation changes dramatically, however, as the V_x integral changes. In particular, the transmission now is restricted within a much narrower energy window around the Fermi energy [see Fig. 14(c)]. A simultaneous variation of E_x and V_x [Fig. 14(d)] produces dramatic shifts in the energy window over which the tube is transmitting. We attribute the rectification properties of the Y tube to this shift.

In the case of model B [Fig. 13(b)], on the other hand, the presence of the hexagonal spacer results in a nonconduction energy window [shown in Fig. 15(a)] in accordance with the results of Treboux *et al*. However, as it is apparent from Fig. 15, the variation of E_x and/or V_x may turn the tube from nonconductive to conductive [see Figs. 15(b) and 15(c)] or may shift the conductive energy window [see Fig. 15(d)]. We attribute, once again, the rectification properties of the Y tubes to this shift. We also note that the behavior of the transmission functions, T_{ij}, in the bottom right panels of Figs. 14 and 15 is very similar to that of the (14,0)-(7,0)-(7,0) Y junction shown in Fig. 2 of Ref. 15 for $E \geqslant E_F$.

As Treboux *et al.* observe, the presented model results are expected to be valid in zigzag Y-shaped SWCNs in an energy

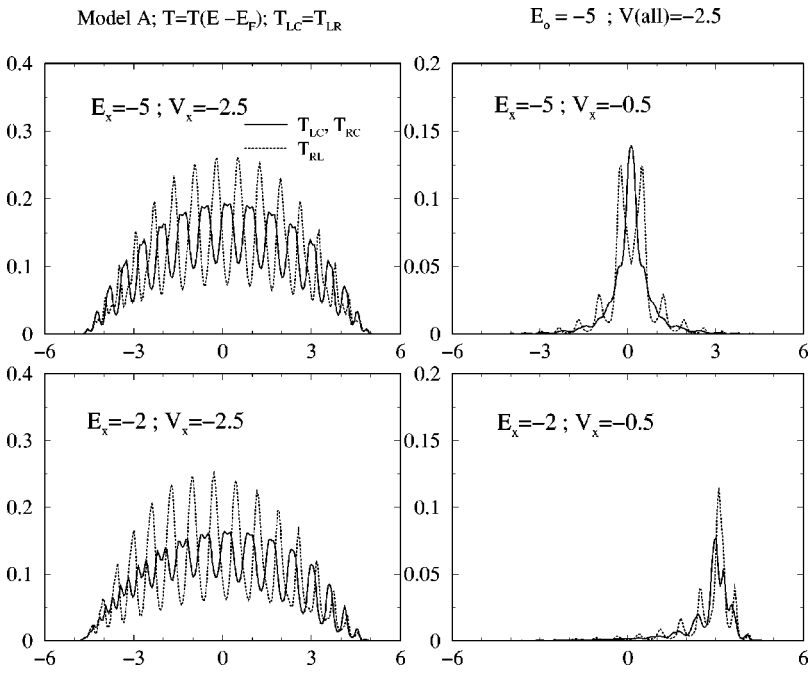

FIG. 14. Results for $T_{ij}(E)$, $i,j=L,R,S$ as a function of energy E, for different E_x and V_x values corresponding to model A [Fig. 13(a)] showing oscillatory features. The spacer consists of a single atom in the middle.

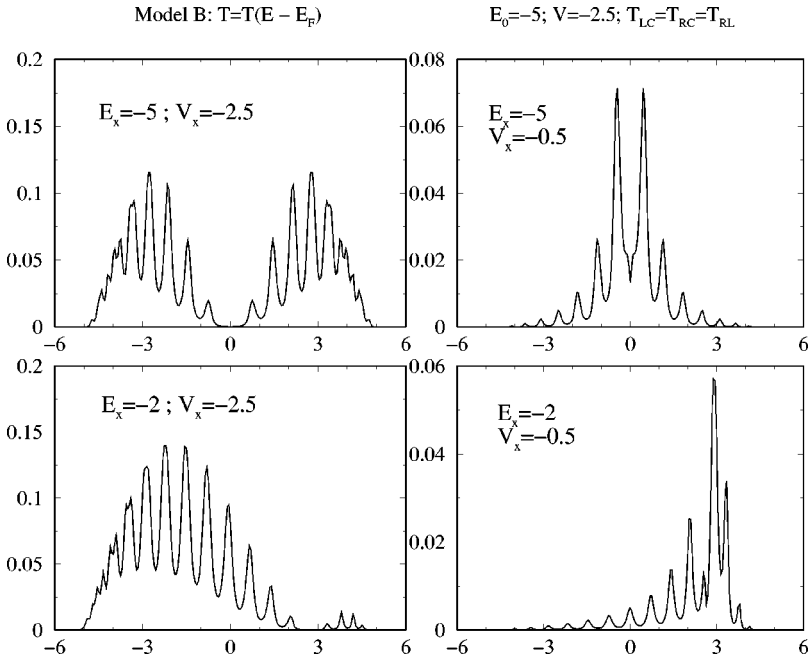

FIG. 15. Results for $T_{ij}(E)$, $i,j=L,R,S$ as a function of energy E, for different E_x and V_x values corresponding to model B [Fig. 13(b)]. The spacer consists of atoms arranged in the form of an hexagon.

window in which they have two conducting channels because these channels belong to the same *E*-irreducible representation of their corresponding group symmetry. From a practical point of view, these results make clear that the Y junctions may be engineered appropriately in order to perform in a desired way.

VII. CONCLUSION

We have presented results of quantum conductivity calculations for various carbon nanotube Y junctions using an efficient Green's-function embedding scheme. The results indicate that rectification and switching properties of these junctions depend strongly on the symmetry and to a lesser degree to chirality suggesting that quantum interference effects are directly influential in rectification. This is further supported by our simple model calculations.

ACKNOWLEDGMENTS

The present paper is supported through grants by NSF (98-62485, NER-0165121, MRSEC Program under award number DMR-9809686), DOE Grant No. (00-63857), NASA grant, and the University of Kentucky Center for Computational Sciences. L.C. acknowledges support from RFBR and RP grants under the title ''Fullerenes and Atomic Clusters''.

APPENDIX: GENERALIZED EULER'S RULE

In this appendix we show the equivalence of Euler's formula with the the consideration proposed by Crespi.

The Euler's formula for polygons on the surface of a closed polyhedron is

$$N(5)-N(7)-2N(8)=12-12G, \tag{A1}$$

where $N(5)$, $N(7)$, and $N(8)$ are the number of pentagons, heptagons and octagons, respectively, and G is the genus (number of holes).[17]

The generalized Euler's rule proposed by Crespi

$$F+V=E+2-2G, \tag{A2}$$

where, F,V, and E, are the number of faces, vertices, and edges, respectively, can be shown to be equivalent to the Euler's formula as follows. Neglecting contributions from all hexagons, the number of faces are given by

$$F=N(5)+N(7)+N(8). \tag{A3}$$

Since each vertex in an sp^2 structure is shared by three polygons,

$$V=[5N(5)+7N(7)+8N(8)]/3. \tag{A4}$$

Similar consideration for the edges leads to

$$E=[5N(5)+7N(7)+8N(8)]/2. \tag{A5}$$

Substituting Eqs. (A3), (A4), and (A5) in Eq. (A2) we obtain Eq. (A1).

*Email address: andriot@iesl.forth.gr
†Email address: super250@pop.uky.edu
‡Email address: deepak@nas.nasa.gov
§Email address: cherno@sky.chph.ras.ru

[1] N. Koprinarov, M. Marinov, G. Pchelarov, M. Konstatinova, and R. Stefanov, J. Phys. Chem. **99**, 2042 (1995).
[2] L. Chico, V.H. Crespi, L.X. Benedict, S.G. Louie, and M.L. Cohen, Phys. Rev. Lett. **76**, 971 (1996).

[3] J.C. Charlier, T.W. Ebbesen, and Ph. Lambin, Phys. Rev. B **53**, 11 108 (1996).
[4] R. Saito, G. Dresselhaus, and M.S. Dresselhaus Phys. Rev. B **53**, 2044 (1996).
[5] M. Menon, D. Srivastava, and S. Saini, *The second NASA Device Modeling Workshop* (NASA Ames, Moffett Field, California, 1997).
[6] L.A. Chernozatonskii, Phys. Lett. A **172**, 173 (1992).
[7] G.E. Scuseria, Chem. Phys. Lett. **195**, 534 (1992).
[8] M. Menon and D. Srivastava, Phys. Rev. Lett. **79**, 4453 (1997).
[9] M. Menon and D. Srivastava, J. Mater. Res. **13**, 2357 (1998).
[10] D. Zhou and S. Seraphin, Chem. Phys. Lett. **238**, 286 (1995).
[11] P. Nagy, R. Ehlich, L.B. Biro, and J. Gjulai, Appl. Phys. A: Mater. Sci. Process. **70**, 481 (2000).
[12] J. Li, C. Papadopoulos, and J. Xu, Nature (London) **402**, 253 (1999).
[13] B.C. Satishkumar, P.J. Thomas, A. Govindraj, and C.N.R. Rao, Appl. Phys. Lett. **77**, 2530 (2000).
[14] C. Papadopoulos, A. Rakitin, J. Li, A.S. Vedeneev, and J.M. Xu, Phys. Rev. Lett. **85**, 3476 (2000).
[15] A.N. Andriotis, M. Menon, D. Srivastava, and L. Chernozatonskii, Phys. Rev. Lett. **87**, 066802 (2001).
[16] A.N. Andriotis, M. Menon, D. Srivastava, and L. Chernozatonskii, Appl. Phys. Lett. **79**, 266 (2001).
[17] V.H. Crespi, Phys. Rev. B **58**, 12 671 (1998).
[18] A.N. Andriotis and M. Menon, J. Chem. Phys. **115**, 2737 (2001).
[19] R. Landauer, Z. Phys. B: Condens. Matter **68**, 217 (1987).
[20] C.M. Soukoulis and E.N. Economou, Waves Random Media **9**, 255 (1999).
[21] J. Bardeen, Phys. Rev. Lett. **6**, 57 (1961).
[22] C. B. Duké, in *Solid State Physics*, edited by F. Seitz, D. Turnbull, and H. Ehrenreich (Academic, New York, 1969).
[23] D.S. Fisher and P.A. Lee, Phys. Rev. B **23**, 6851 (1981).
[24] S. Datta, in *Electronic Transport in Mesoscopic Systems* (Cambridge University, Cambridge, England, 1995).
[25] See paragraph 3.7 of Ref. 24.
[26] M.P. Samanta, W. Tian, S. Datta, J.I. Henderson, and C.P. Kubiak, Phys. Rev. B **53**, R7626 (1996).
[27] M.B. Nardelli, Phys. Rev. B **60**, 7828 (1999).
[28] M.P. Anantram and T.R. Govindan, Phys. Rev. B **58**, 4882 (1998).
[29] M. Menon and R.E. Allen, Phys. Rev. B **33**, 7099 (1986); *ibid.* **38**, 6196 (1988).
[30] M. Menon, N.N. Lathiotakis, and A.N. Andriotis, Phys. Rev. B **56**, 1412 (1997).
[31] R.E. Allen and M. Menon, Phys. Rev. B **33**, 5611 (1986).
[32] J.E. Inglesfield, J. Phys. C **14**, 3795 (1981).
[33] G.A. Baraff and M. Schluter, J. Phys. C **19**, 4383 (1986).
[34] A.N. Andriotis, Europhys. Lett. **17**, 349 (1992); A.N. Andriotis, J. Phys.: Condens. Matter **2**, 1021 (1990).
[35] A.J. Fisher, J. Phys.: Condens. Matter **2**, 6079 (1990).
[36] J.-C. Charlier, Ph. Lambin, and T.W. Ebbesen, Phys. Rev. B **54**, R8377 (1996).
[37] M. Buttiker, IBM J. Res. Dev. **32**, 317 (1988).
[38] M.B. Nardelli and J. Bernholc, Phys. Rev. B **60**, R16 338 (1999).
[39] S. Sanvito, C.J. Lambert, J.H. Jefferson, and A.M. Bratkovsky, Phys. Rev. B **59**, 11 936 (1999).
[40] W. Harrison, in *Electronic Structure and Properties of Solids* (W. H. Freeman, San Francisco, 1980).
[41] A.N. Andriotis, M. Menon, G. Froudakis, and J.E. Lowther, Chem. Phys. Lett. **301**, 503 (1999).
[42] E.G. Emberly and G. Kirczenow, Phys. Rev. B **58**, 10 911 (1998).
[43] A.A. Farajian, K. Esfarjani, and Y. Kawazoe, Phys. Rev. Lett. **82**, 5084 (1999).
[44] A.N. Andriotis and M. Menon, Phys. Rev. B **59**, 15 942 (1999).
[45] W. Tian, S. Datta, S. Hong, R. Reifenberger, J.I. Henderson, and C.P. Kubiak, J. Chem. Phys. **109**, 2874 (1998).
[46] L.E. Hall, J.R. Reimers, N.S. Hush, and K. Silverbrook, J. Chem. Phys. **112**, 1510 (2000).
[47] K. Hieke and M. Ulfward, Phys. Rev. B **62**, 16 727 (2000).
[48] M. Menon, E. Richter, and K.R. Subbaswamy, J. Chem. Phys. **104**, 5875 (1996).
[49] M. Menon and K.R. Subbaswamy, Phys. Rev. B **55**, 9231 (1997).
[50] A.N. Andriotis and M. Menon, Phys. Rev. B **60**, 4521 (1999).
[51] A.N. Andriotis, M. Menon, and G.E. Froudakis, Phys. Rev. B **62**, 9867 (2000).
[52] M. Menon, A.N. Andriotis, and G.E. Froudakis, Chem. Phys. Lett. **320**, 425 (2000).
[53] A.N. Andriotis, M. Menon, and G.E. Froudakis, Phys. Rev. B **61**, R13 393 (2000).
[54] A.N. Andriotis, M. Menon, and G.E. Froudakis, Phys. Rev. Lett. **85**, 3193 (2000).
[55] G. Froudakis, A.N. Andriotis, and M. Menon, Chem. Phys. Lett. **350**, 393 (2001).
[56] T. Palm and L. Thylen, J. Appl. Phys. **79**, 8076 (1996).
[57] H.Q. Xu, Appl. Phys. Lett. **78**, 2064 (2001).
[58] A.M. Song, A. Lorke, A. Kriele, J.P. Kotthaus, W. Wegscheider, and M. Bichler, Phys. Rev. Lett. **80**, 3831 (1998).
[59] A.M. Song, Phys. Rev. B **59**, 9806 (1999).
[60] J-O.J. Wesstrom, Phys. Rev. Lett. **82**, 2564 (1999).
[61] G. Treboux, P. Lapstun, Z. Wu, and K. Silverbrook, J. Phys. Chem. B **103**, 8671 (1999).